BIOLOGICA NYSSANA
16 (1) June 2025: 233-245
DOI: 10.46793/BiolNyss.16.1.18Y

Isolation, characterization, *in silico* docking, and *in vitro* cytotoxicity study of isolated triterpene constituents from *Ehretia microphylla*

Original Article

Ramakrishnan Yuvaraja
Department of Pharmaceutical Chemistry, KTN College of Pharmacy, Chalavara, Kerala, India

Kullampalayam Krishnasamy Sivakumar
Department of Pharmaceutical Chemistry, Sri Venkateshwara College of Pharmacy, Ariyur, Pondicherry, India
sivakumarkk1174@gmail.com (corresponding author)

Santhiagu Arockiasamy
Bioscience and Engineering, NIT Calicut, Kerala, India

Jayaraman Rajangam
Department of Pharmaceutical Chemistry, Sri Venkateshwara College of Pharmacy, Ariyur, Pondicherry, India

Arulkumaran Govindarajan
Department of Pharmaceutical Chemistry, KTN College of Pharmacy, Chalavara, Kerala, India

Received: December 16, 2024
Revised: April 08, 2025
Accepted: April 14, 2025

Abstract:

Building on previous studies of *Ehretia microphylla*, we quantified key phytochemicals rutin, gallic acid, and quercetin using high-performance thin-layer chromatography (HPTLC), validated against standard references. From chloroform extract, three triterpenes were isolated and structurally characterized. These were identified as bauerenol (Compound A), 11-oxo amyrin (Compound B, a novel triterpene), and *β*-sitosterol (Compound C). *In silico* docking studies were performed with the cancer-related protein (PDB: 1DB1), yielding binding scores of −9.50, −9.44, and −7.44, and with the hepatoprotective target (PDB: 4FA6), with scores of −8.13, −8.42, and −8.54, respectively. Compounds A and B exhibited significant anticancer potential, while Compound C showed superior hepatoprotective activity. *In vitro* cytotoxicity studies on HepG2 cells revealed IC_{50} values of 455, 538, and 556 µg/mL, and on NIH 3T3 cells, IC_{50} values were 1068, 1153, and 1310 µg/mL, indicating selective toxicity toward cancer cells. These findings highlight the therapeutic potential of triterpenes from *E. microphylla*, with Compounds A and B for hepatocellular carcinoma treatment and Compound C for hepatoprotection.

Key words:
Ehretia microphylla, triterpenes, hepatoprotective, cytotoxicity, docking studies

Apstrakt:

Izolacija, karakterizacija, *in silico* dokovanje i *in vitro* ispitivanje citotoksičnosti triterpenskih jedinjenja izolovanih iz *vrste Ehretia microphylla*

Nadovezujući se na prethodna istraživanja vrste *Ehretia microphylla*, kvantifikovali smo rutin, galnu kiselinu i kvercetin, primenom HPTLC metodologije. Iz hloroformskog ekstrakta izolovana su i identifikovana tri triterpenska jedinjenja: bauerenol (jedinjenje A), 11-okso-amirin (B, novi triterpen) i *β*-sitosterol (C). *In silico* dokovanja pokazala su afinitete ka ključnim proteinima povezanim sa karcinomom (PDB: 1DB1), sa rezultatima dokovanja -9.50, -9.44 i -7.44, kao i sa hepatoprotektivnim ciljnim proteinom (PDB: 4FA6), sa skorovima -8.13, -8.42 i -8.54. Jedinjenja A i B ispoljila su izražen antiproliferativni potencijal, dok je C pokazalo superiornu hepatoprotektivnu aktivnost. *In vitro* testiranja na HepG2 ćelijama pokazala su IC_{50} vrednosti od 455, 538 i 556 µg/mL, a na NIH 3T3 ćelijama IC_{50} vrednosti od 1068, 1153 i 1310 µg/mL, ukazujući na selektivnu citotoksičnost prema ćelijama kancera. Dobijeni rezultati potvrđuju terapijski potencijal triterpena vrste *E. microphylla*, sa jedinjenjima A i B perspektivnim za lečenje hepatocelularnog karcinoma i jedinjenjem C za hepatoprotektivno dejstvo.

Ključne reči:
Ehretia microphylla, triterpeni, hepatoprotektor, citotoksičnost, dokovanje

Introduction

Cancer is a general term for a large group of diseases that can affect any part of the body. Under normal circumstances, cells grow and die in a regulated manner; however, cancer cells grow uncontrollably and evade programmed cell death. Cancer is the second leading cause of mortality worldwide, following cardiovascular diseases (Sharma et al., 2022). Among the various types of cancer globally,

the most common form of primary liver cancer is hepatocellular carcinoma (HCC), also known as hepatoma, which ranks fourth in the world in terms of cancer-related deaths (Villanueva, 2019). According to annual projections, the World Health Organization estimates that more than one million patients will die from liver cancer by 2032 (World Health Organization, 2016). Liver cancer cells are primarily hepatocytes and are often a complication of cirrhosis, which can be caused by Hepatitis B or C virus infections or prolonged alcohol consumption. Efforts to control liver cancer have significantly benefited from research into medicinal plants.

Traditional cancer treatment approaches include surgery, radiation therapy, targeted therapy, immunotherapy, hyperthermia, stem cell transplantation, photodynamic therapy, laser therapy, blood product donation, transfusion, and, most importantly, chemotherapy (Maurya, 2014). However, despite the wide variety of synthetic drugs used in cancer chemotherapy and the therapeutic successes of various treatment regimens, the prevailing therapies have not always yielded the expected results. Tumor relapse and metastasis frequently occur, necessitating further research into alternative and complementary therapies. There is a growing need for natural, selective active compounds with fewer side effects, lower costs, and more medicinal properties. Compounds with minimal disease resistance are particularly crucial for cancer treatment, especially those derived from biological and natural sources (Sharifi-Rad et al., 2019). One such plant is *Ehretia microphylla* Lam. (EM), which has been reported to contain numerous bioactive metabolites, including triterpenes, alkaloids, glycosides, tannins, *α*-amyrin, *β*-amyrin, saponins, flavonoids, and rosmarinic acid (Aarthi et al., 2014; Pooja et al., 2022; Jiang et al., 2024). This plant, belonging to the Boraginaceae family, is of significant medicinal value in the Philippines and other Asian countries. Traditionally, EM has been used in the form of a decoction to treat coughs, diarrhea with bloody discharge, and dysentery. Scientific studies have also reported its antioxidant, antimicrobial, anti-hypercholesterolemic, and anti-allergic activities (Palaniappan et al., 2014; Umali et al., 2014; Cagampan et al., 2018).

Various phytochemical constituents, which possess a steroid nucleus, play a crucial role in hepatoprotective and anticancer activities. An example of such a compound is vitamin D. Vitamin D also plays a crucial role in regulating the phosphatidylinositol 3-kinase alpha (PI3Kα) pathway (Yuan et al., 2021; Shamsan et al., 2024), which is vital for cell growth, survival, and metabolism. Dysregulation of the PI3Kα pathway is implicated in various liver diseases (e.g., non-alcoholic fatty liver disease, fibrosis, and cirrhosis) as well as in cancer, making vitamin D a promising therapeutic agent for the prevention and management of these conditions. In liver disease, vitamin D's active form, calcitriol, modulates the PI3Kα pathway (Trump, 2018) to reduce inflammation, prevent fibrosis, and promote liver regeneration. It inhibits the activation of hepatic stellate cells (HSCs), which are responsible for collagen production and liver scarring. By suppressing the PI3Kα/Akt signalling pathway, vitamin D reduces the activation of HSCs, potentially slowing or reversing liver fibrosis progression (Chen et al., 2022). Moreover, vitamin D regulates inflammatory cytokines such as TNF-α and IL-6, which contribute to liver injury, further supporting its hepatoprotective effects.

In cancer, particularly liver cancer (HCC), vitamin D interferes with PI3Kα signalling to inhibit tumor growth and metastasis. Calcitriol can induce apoptosis in cancer cells and prevent their proliferation by modulating the PI3K/Akt pathway (Chiang & Chen, 2011; Zhang et al., 2020). It also reduces epithelial-to-mesenchymal transition (EMT), a key step in cancer metastasis. Additionally, vitamin D enhances immune surveillance by promoting the activity of immune cells like T cells and natural killer (NK) cells, which are involved in targeting and eliminating tumor cells. Interestingly, the phytochemical constituents of *E. microphylla* extract have structures resembling steroids (such as the cyclopentanoperhydrophenanthrene ring structure), similar to vitamin D. Overall, vitamin D's modulation of PI3Kα offers dual protective effects in both liver diseases and cancer, influencing inflammation, fibrosis, cell survival, and metastasis.

In continuation of our research on *E. microphylla* (Yuvaraja et al., 2020; Yuvaraja et al., 2021), we report the quantification of major phytochemicals like rutin, gallic acid, and quercetin using high-performance thin-layer chromatography (HPTLC). We also isolated three triterpene compounds from chloroform extracts of *E. microphylla* and characterized their structures. *In silico* docking, ADME studies were conducted on these isolated triterpene constituents, focusing on key transcription factors involved in hepatocellular carcinoma (HCC). Additionally, we explored the *in vitro* cytotoxicity of these compounds against HepG2 (human hepatoma) and NIH 3T3 (mouse embryonic fibroblast) cell lines using the MTT assay.

Materials and Methods

Collection of plant parts and instrumentation

Based on the literature review and traditional claims,

aerial parts of *E. microphylla* were collected locally in Sattankulam at Thoothukudi District in Tamil Nadu from June to August. The collected plants were authenticated by the Survey of Medicinal and Aromatic Plants Unit Siddha, Central Council for Research in Ayurvedic Sciences (CCRAS), Palayamkottai, Tamil Nadu, India.

Borosil glassware was used throughout the entire project. They were soaked in chromic acid for 3 days, washed with tap water, rinsed with distilled water, and dried in a hot air oven. Analytical grade chemicals supplied by SD Fine Chemicals, SRL, Hi Media, Merck India, and Sigma Aldrich Chemicals were used for this research. Instruments like analytical weighing balance (Shimadzu-AUW220D, Shimadzu Corporation, Kyoto, Japan), High-Performance Layer Chromatography (HPLC), (CAMAG Linomat 5 with TLC Scanner 3, CAMAG, Muttenz, Switzerland), FT-IR (JASCO FT/IR-4100 JASCO Corporation, Tokyo, Japan), NMR (Bruker Avance III 400 MHz, Bruker BioSpin GmbH, Rheinstetten, Germany), GC-MS (PerkinElmer Clarus 500 GC-MS, PerkinElmer Inc., Waltham, MA, USA) were used. The human hepatoma cell line (HepG2) and mouse embryonic fibroblasts cell line (NIH 3T3) were obtained from the National Centre for Cell Science (NCCS), Pune. Cells were maintained at 370 °C, 5% CO_2, 95% air, and 100% relative humidity. Maintenance cultures were passaged weekly, and the culture medium was changed twice a week.

Quantitative estimation of major phytochemicals by HPTLC method

The collection of plant material, extraction method, solvent system, percentage yield of extracts, identification, and quantitative phytochemicals were evaluated and reported. Based on the earlier research, major phytochemicals present in the chloroform *E. microphylla* extract (CEM) and ethyl acetate extract (EAEM) were quantitatively estimated by the HPTLC method (Sajeeth et al., 2010).

Preparation of standard and sample solutions

Stock solutions of standard compounds were prepared by dissolving 100 mg of gallic acid, rutin, and quercetin in 100 mL of methanol (HPTLC grade). 1000 mg of CEM and EAEM extract were dissolved in 100 mL of methanol, filtered using Whatman No.1 filter paper, and stored in an amber-colored container at 4 °C.

Procedure for extraction of active constituents

Five microliters of gallic acid, rutin, quercetin, and extracts were spotted in the form of bands with a microliter syringe on pre-coated silica gel glass plate 60 F_{254} (10×10 cm with 0.2 mm thickness) using a Camag Linomat 5 applicator. The plates were pre-washed with methanol and activated at 60 °C for 10 min before chromatography. After chamber saturation with the respective mobile phase, the sample-loaded plate was kept in a TLC twin trough developing chamber. The optimized chamber saturation time for the mobile phase was 5 min at room temperature. Linear ascending development was carried out, and the plate was developed in the respective mobile phase up to 7 cm. The developed plate was then dried by hot air to evaporate solvents from the plate and develop bands. The dried plate was observed under UV light at 254 nm and 366 nm, and photo documentation was done. Densitometric scanning was performed on Camag TLC scanner 3 in the absorbance mode at 280 nm. The percentage of active constituents present in the chloroform and ethyl acetate extracts was compared with that of the standard (Jain et al., 2006; Jeganathan & Kannan, 2008).

Isolation of triterpene constituents from CEM by column chromatography

Based on the results obtained from phytochemical screening and TLC studies, the solvent system was selected for column chromatography using the isocratic elution technique (Mahrath et al., 2015; Mawa et al., 2016). The silica gel (60-120 mesh) was made into a suspension with the selected solvent system (chloroform:ethyl acetate). Silica gel was pre-activated by heating in a hot air oven at 100 °C for 1 h. The bottom of the column was plugged with cotton, and then the silica gel slurry was poured into the column, which was filled with a solvent system to a height of 50 cm. After that, it was set aside for 10 min and allowed to settle. The CEM was mixed with a small amount of silica gel and moistened with a solvent system, mixed well, and allowed to evaporate the solvent to get the dry residue. Then, the dry residue was charged on the column with the help of a solvent system; after that, cotton was placed over it to avoid the disturbance of the top layer of the adsorbent, as a fresh mobile phase was added to the column.

Spectral data of Isolated compounds

Compound A: (Bauerenol): IUPAC Name: 4, 4, 6b, 8a, 11, 12, 12b, 14b-octamethy l-1, 2, 3, 4, 4a, 5, 6b, 7, 8, 8a, 9, 10, 11, 12, 12a, 12b, 13, 14, 14a, 14b-icosahydropicen-3-ol; MP: 278-283 °C; UV: 217; IR (KBr, cm^{-1}): 3384 (OH stretch), 2962, 2917 (ali-cyclic -CH_2 stretch), 2894 (alicyclic -CH- stretch), 1655 (C=C stretch); ^{1}H NMR (DMSO-d_6) δ ppm: 0.74 to 1.39 (s, 24H, methyl -CH_3, no resolved J

value) 1.46 to 1.95 (s, 18H, -CH_2-CH_2- ethylene), 1.48 to 1.59 (s, 6H, CH of methylene), 3.24 (d, 1H , =CH, J= 10.5 Hz), 5.152 (s, 1H, hydroxyl -OH); ^{13}C NMR: δ 145.35, 116.44, 79.06, 77.41, 56.22, 54.89, 50.41, 48.22, 41.23, 39.65, 38.77, 37.69, 36.88, 35.33, 35.20, 32.42, 32.04, 31.52, 29.70, 28.87, 27.68, 27.53, 25.63, 24.15, 23.66, 22.66, 22.55, 16.80,14.66, 12.98; Exact Mass: *m/z*: 426.72 $[M]^+$; Chemical Formula: $C_{30}H_{50}O$; Calculated elemental analysis: C- 84.44%; H- 11.81%; O- 3.75%.

Compound B: (11-Oxo-Aamyrin): IUPAC Name: 10-hydroxy-1,2,4a,6a,9,9,12a-heptamethyl-1,3,4,4a,5,6,6a,6b,7,8,8a,9,10,11,12,12a,12b,14b-octadecahydropicen-13(2H)-on. MP: 280 – 285 °C; UV: 218; IR (KBr, cm^{-1}): 3312 (-OH stretch), 2944 (alicyclic -CH_2 stretch), 2857 (alicyclic -CH- stretch), 1716 (C=O stretch).^{1}H NMR (DMSO-d_6) δ ppm: 0.81 to 1.25 (s, 24H, methyl -CH_3 no resolved J value), 1.27 to 1.55 (s, 16H, -CH_2-CH_2- ethylene), 1.55to 1.64 (s, 6H, CH of methylene), 3.27 (d 1H, =CH), 5.184 (s, 1H, hydroxyl -OH); ^{13}C NMR: δ 200.13, 175.16, 129.26, 116.44, 79.27, 77.42, 71.81, 56.85, 55.94, 45.82, 42.34, 40.48, 39.67, 37.24, 36.14, 33.93, 31.89, 31.65, 28.91, 28.24, 26.06, 25.39, 24.29, 23.05, 20.12, 20.01, 19.81, 17.68, 16.43, 15.65; Exact Mass: *m/z*: 440.37 $[M]^+$; Chemical formula $C_{30}H_{48}O_2$; Calculated elemental analysis: C- 81.76%; H- 10.98%; O- 7.26.%

Compound C: (β-Sitosterol): IUPAC Name: 17-(5-ethyl-6-methylheptan-2-yl)-10, 13-dimethyl-2, 3, 4, 7, 8, 9, 10, 11, 12, 13, 14, 15, 16, 17- tetradecahydro-1H cyclopenta[a]phenanthren-3-ol; MP: 135–136.5 °C; UV 220: IR (KBr, cm^{-1}): 3100–3400 (-OH stretch), 2912 (alicyclic -CH_2 stretch), 1379, 1465 (alicyclic -CH- stretch); ^{1}H NMR (DMSO-d_6) δ ppm: 0.69 to 1.08 (s, 18H, methyl -CH_3), 1.12 to 1.81 (s, 22H, -CH_2-CH_2- ethylene), 1.53 to 1.99 (s, 8H, CH of methylene), 3.52 (d 1H , =CH), 5.36 (s, 1H, hydroxyl -OH); ^{13}C NMR: δ 140.75, 138.31, 121.71, 56.87, 56.77, 51.23, 45.84, 42.29, 40.48, 39.78, 37.25, 36.51, 36.14, 33.95, 33.71, 32.41, 31.90, 31.65, 29.16, 28.91, 28.24, 26.09, 25.40, 24.36, 23.07, 23.05, 21.20, 21.07, 12.28; Exact Mass: *m/z*: 397$[M]^+$; Chemical formula: $C_{29}H_{50}O$; Calculated elemental analysis: C- 83.99%; H- 12.15%; O- 3.86%.

Cytotoxicity study by MTT assay

Cells were maintained at 37 ºC, 5% CO_2, 95% air, and 100% relative humidity. Maintenance cultures were passaged weekly, and the culture medium was changed twice a week. A mitochondrial enzyme in living cells, succinate-dehydrogenase, cleaves the tetrazolium ring, converting the MTT to an insoluble purple formazan. Therefore, the amount of formazan produced is directly proportional to the number of viable cells (Mosmann, 1983; Monks et al., 1991). After 48 h of incubation, 15 µl of MTT (5 mg/mL) in phosphate-buffered saline (PBS) was added to each well and incubated at 37 °C for 4 h. The medium with MTT was then flicked off, and the formed formazan crystals were solubilized in 100 µl of DMSO and then the absorbance was measured at 570 nm using a microplate reader. The % cell inhibition was determined using the following formula:

$$\% \text{ cell inhibition} = 100 - \text{Abs (sample)}/\text{Abs (control)} \times 100$$

A nonlinear regression graph was plotted between % cell inhibition and Log_{10} concentration, and IC_{50} was determined using GraphPad Prism software.

Ligand docking and ADME properties screening

Docking study is an online server for performing site-specific molecular docking. The target PDB: 1DB1 & 4FA6 were uploaded, and the binding site for the ligand was specified by clicking on the "Select binding center" button. The binding center was selected by opening the target visualizer, which will be considered as the isolated compounds A, B, and C, which were the geometric center of the binding center. The data, such as Name, PDB ID, Uniprot Name, Uniprot Accession ID/ Taxonomic ID, Organism, and resolution, were specified. The binding site in angstroms is set according to the size of the ligand, which typically covers a sufficiently large space for docking of the small molecule. The maximum number of binding modes and exhaustiveness were specified. This server uses Autodock Vina for docking calculations. Ligands are ranked by using docking scores (the more negative, the better), which suggests how properly the ligand is anticipated to bind to the target. It is, however, also important to check the binding mode and analyze whether it is in agreement with active site residues (https://mcule.com/apps/1-click docking/).

Results and discussion

Isolation and structure characterization

The HPTLC study demonstrated that both extracts contain rutin, gallic acid, and quercetin. The R_f value of *E. microphylla* extracts and standard specimens, rutin, gallic acid, and quercetin were presented in **Tab. 1**. Detection of bands at UV light 254 nm and the densitograms are offered in **Fig. 1** and **Fig. 2**, respectively. The HPTLC results proved that the R_f values of specimen rutin, gallic acid, and quercetin are 0.18, 0.78, and 0.87, respectively. Totally 9 spots were obtained in the chloroform extract. Among the 9 spots of the chloroform extract, the R_f value of spot 2 is 0.18, which matches the R_f of standard rutin.

Table 1. Rf values of CEM and EAEM, and standard markers

Peak	Name of the formulation/ Volume (5.0 µL)					
	Track-1 (CEM)			Track-2 (EAEM)		
	R_f value of peak	Area of peak	Assigned substance	R_f value of peak	Area of peak	Assigned substance
1	0.01	3818.3	unknown	1.01	1271.9	unknown
2	**0.18**	**15297.8**	**Rutin**	0.11	4695.9	unknown
3	0.26	609.5	unknown	**0.18**	**17477.3**	**Rutin**
4	0.33	149.2	unknown	0.25	894.8	unknown
5	0.43	689.2	unknown	0.42	1880.4	unknown
6	0.49	322.2	unknown	0.58	1172.1	unknown
7	0.57	1072.4	unknown	0.63	12808.1	unknown
8	**0.78**	**19300.4**	**Gallic acid**	**0.78**	**22882.4**	**Gallic acid**
9	**0.87**	**15130.9**	**Quercetin**	**0.87**	**18758.3**	**Quercetin**

Standard/Volume (5.0 µL)	Peak	R_f value of peak	Area of peak	Assigned substance
Track-3 (Rutin)	1	0.18	58576.5	Rutin
Track-4 (Gallic acid)	1	0.78	54563.7	Gallic acid
Track-5 (Quercetin)	1	0.87	48339.1	Quercetin

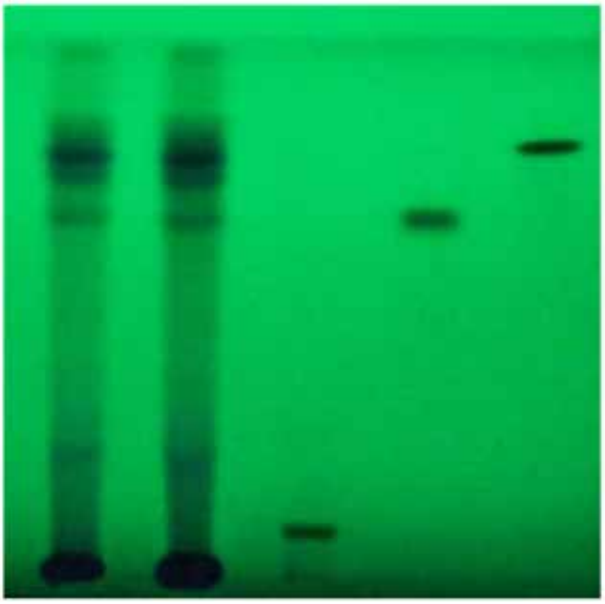

Fig. 1. Detection of bands at UV light 254 nm - Track 1: CEM, Track 2: EAEM, Track 3: Rutin, Track 4: Gallic acid, and Track 5: Quercetin

The R_f value of the 8th spot is 0.78, which exactly matches the R_f value of standard gallic acid, and the R_f value of spot 9 is 0.87, which is the R_f value of standard quercetin. Also, a total of 9 spots are obtained in the chromatogram of EAEM. Among the 9 spots of EAEM, the Rf values of 3, 8, and 9 spots are 0.18, 0.78, and 0.87, respectively, which indicate the presence of rutin, gallic acid, and quercetin, respectively. The quantification of the identified compounds (rutin, quercetin, and gallic acid) present in CEM and EAEM was calculated by using the peak area of the extracts CEM and EAEM and is given in **Tab. 2**. The results revealed that EAEM showed the presence of a higher amount of rutin, gallic acid, and quercetin compared with CEM.

The chloroform extract was subjected to silica gel column chromatography. The solvent system used for the chromatographic analysis of CEM was presented in **Tab. 3**. The column was eluted with the selected solvent system by the isocratic method and the fractions were collected in a clean 100 mL beaker up to 25 mL at a speed of 25 drops/min. Each collected fraction was tested for the presence of various constituents by TLC for the number and types of constituents, and similar fractions were pooled together. The migration of spot-on chromatograms is indicated by the term R_f value. The fractionated compounds A, B, and C were subjected to TLC analysis and characterized by various spectral analyses (UV, IR, Mass, and NMR spectroscopy).

The fractionated compounds A, B, and C were presented in **Fig. 3**. The IR spectrum of isolated compound A displayed -OH stretch at 3384 cm^{-1},

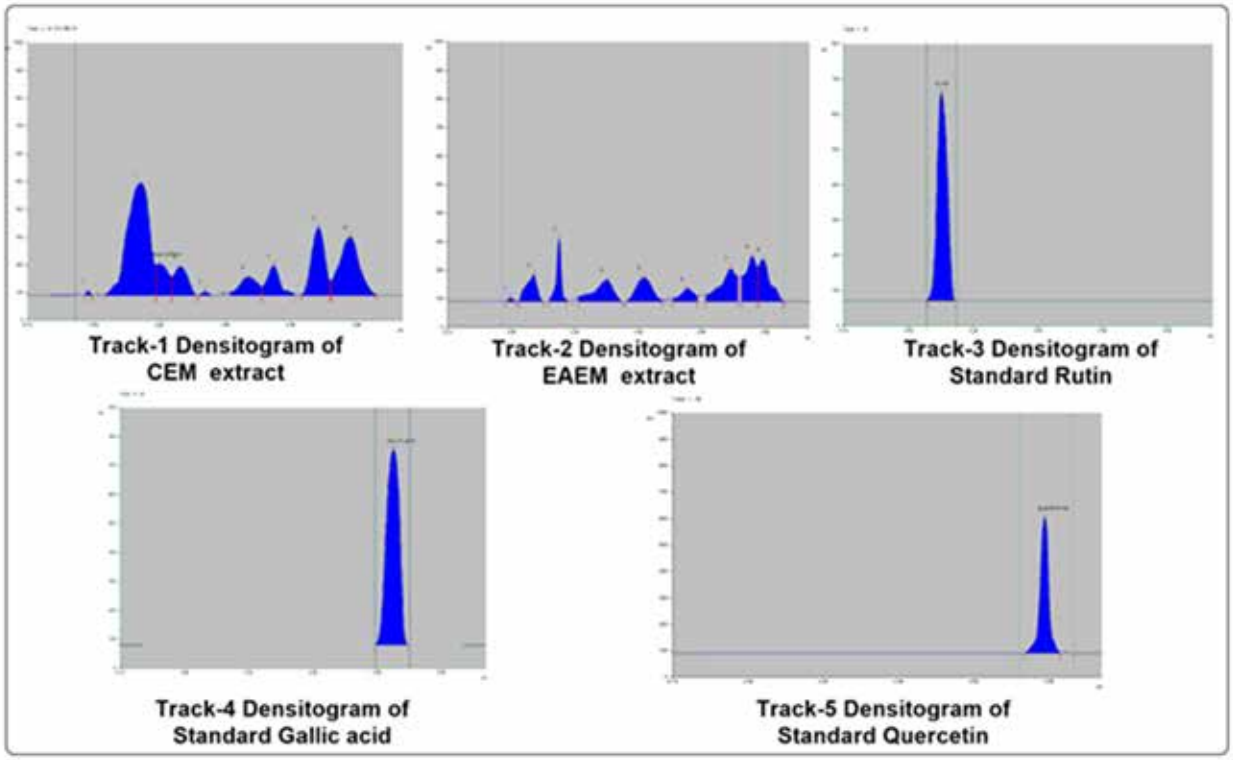

Fig. 2. Densitograms display of the standard and extracts

Table 2. Quantification of identified compounds in CEM and EAEM using HPTLC

S. No	Track	Sample	Volume (µl)	Rutin (1 mg/ml) of extract (%)	Gallic acid (1 mg/ml) of extract (%)	Quercetin (1 mg/ml) of extract (%)
1	Track-1	CEM	5.0	0.4394	0.2774	0.2890
2	Track-2	EAEM	5.0	1.2550	0.4522	0.6613

Table 3. Solvent profile for column chromatography of fractionated compounds

Compounds	Solvent system	Solvent ratio
A	Chloroform: Methanol: Acetic acid	15:8:3:2
B	Chloroform: Methanol: Water	15:3:1
C	Toluene: Ethyl acetate: Glacial acetic acid	8: 2: 0.2

-CH_2 stretch at 2962 cm^{-1} and 2917 cm^{-1}, alicyclic -CH- stretch at 2894 cm^{-1}, and C=C stretch at 1655 cm^{-1}, indicating the presence of these functional groups in compound A. The IR spectrum of fractionated compound B exhibited a stretch at 3312 cm^{-1}, which indicates the presence of a hydrogen-bonded OH group. The prominent absorption at 2944 cm^{-1} indicates CH_2 stretching vibration due to the alicyclic ring. The band at 2857 cm^{-1} is considered for the alicyclic CH stretch. The wide band at 1716 cm^{-1} indicates C=O stretching. Fractionated compound C showed an IR spectrum band in a wide range of 3100-3400 cm^{-1}, indicating the OH stretch's presence in the compound. The stretch at 2912 cm^{-1} indicates the presence of the alicyclic CH_2 group, and the bands at 1379, 1465 cm^{-1} are consistent with the alicyclic CH stretch.

The interpretation of all the spectral studies gives the tentative possible structure of compounds A, B, and C. Compound A is bauerenol ($C_{30}H_{50}O$) [triterpene alcohol], compound B is 11-oxo-amyrin ($C_{30}H_{48}O_2$), and compound C was *β*-sitosterol ($C_{29}H_{50}O$). Compounds A and C were previously reported in *E. microphylla*, and to the best of our knowledge, compound B is isolated for the first time from *E. microphylla*.

Compound A

The ^{1}H-NMR spectrum of compound A indicated the presence of 50 protons. Multiple singlets observed

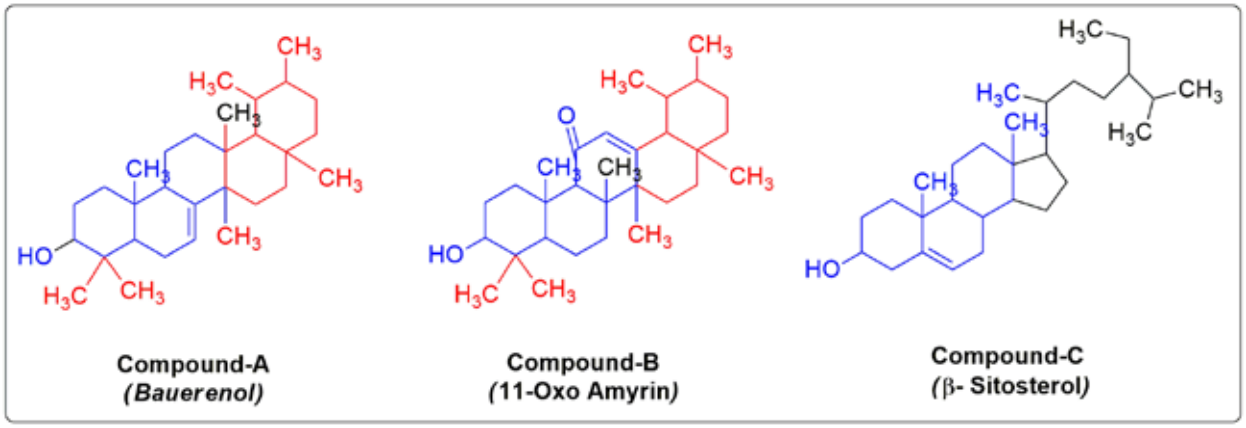

Fig. 3. Compounds isolated from *Ehretia microphylla* aerial parts

between δ 0.74–1.39 ppm corresponded to 24 methyl protons, suggesting the presence of eight methyl groups, typical in highly substituted triterpenoid or steroidal structures. Signals between δ 1.46–1.95 ppm (18H) and δ 1.48–1.59 ppm (6H) were assigned to methylene and methine protons, respectively. A doublet at δ 3.24 ppm (1H) suggested a vinylic proton, and a singlet at δ 5.152 ppm (1H) indicated a hydroxyl group.

The ^{13}C-NMR spectrum revealed 30 carbon atoms: 8 CH_3, 9 CH_2, 7 CH, and 6 quaternary carbons. Notably, downfield signals at δ 145.35 and 116.44 ppm suggested the presence of an alkene moiety, while the resonance at δ 79.06 ppm was consistent with a carbon bearing a hydroxyl group. This spectral profile is consistent with a tetracyclic triterpenoid backbone bearing oxygenated functionalities.

Compound B

Compound B was found to contain 48 protons and 30 carbon atoms. Its ^{1}H-NMR spectrum exhibited singlets between δ 0.81–1.25 ppm (24H), indicating the presence of eight methyl groups. The singlets at δ 1.27–1.55 ppm (16H) and δ 1.55–1.64 ppm (6H) were attributed to methylene and methine protons, respectively. Similar to compound A, a doublet at δ 3.27 ppm (1H) represented a vinylic proton, while the signal at δ 5.184 ppm (1H) corresponded to a hydroxyl group. The ^{13}C-NMR spectrum also confirmed a 30-carbon framework comprising 8 CH_3, 8 CH_2, 7 CH, and 7 quaternary carbon atoms. The signal at δ 200.13 ppm indicated the presence of a carbonyl group, most likely a ketone, while δ 175.16 ppm suggested a carboxylic or ester carbon. The alkene carbons (δ 129.26 and 116.44 ppm), along with hydroxyl-bearing carbons (δ 79.27 and 71.81 ppm), highlighted the oxygenated and unsaturated nature of the compound. The presence of both ketone and carboxylic functionalities, along with olefinic and hydroxyl groups, suggests that compound B is more oxidized than compound A. The variations in quaternary carbon content also reflect a structural rearrangement, possibly due to oxidation or skeletal modifications.

Compound C

Compound C exhibited 50 protons and 29 carbon atoms, slightly fewer than compounds A and B. The ^{1}H-NMR spectrum revealed δ 0.69–1.08 ppm (18H) from six methyl groups, δ 1.12–1.81 ppm (22H) attributed to methylene protons, δ 1.53–1.99 ppm (8H) corresponding to methine protons, δ 3.52 ppm (1H, doublet) as vinylic hydrogen, δ 5.36 ppm (1H, singlet) indicating a hydroxyl proton.

The range δ 0.74–1.39 ppm in the ^{1}H NMR of bauerenol corresponds to methyl protons (CH_3), most of which appear as singlets or pseudo-doublets in highly symmetrical triterpenes like bauerenol. Here, an NMR signal was observed at δ 0.74–1.39 ppm as a singlet (s, 24H, CH_3), and no resolvable J-coupling was detected. Methyl groups attached to quaternary or tertiary carbons usually appear as singlets because they do not couple significantly with neighboring protons. If attached to methylene (CH_2) or methine (CH), the coupling may occur, but in rigid triterpenoid structures, it's often too small to resolve. On the other hand, because it's a multiplet signal 1.46-1.95 m (m, 18H, CH_2), these protons likely experience overlapping couplings from neighboring protons in a rigid framework; no single J can define the whole group. The ^{13}C-NMR data revealed 6 CH_3, 11 CH_2, 9 CH, and 3 quaternary carbons. The relatively high number of CH_2 and CH carbons, along with fewer quaternary centers, suggests a more linear or less fused-ring structure compared to A and B. The signals at δ 140.75, 138.31, and 121.71 ppm point to the presence of a double bond system, possibly part of a substituted olefinic chain. Moreover, the lower number of quaternary carbons and the absence of carbonyl peaks in compound C suggest a less oxygenated framework, indicating that compound C may represent a precursor or a

reduced form relative to A and B.

In silico screening and biological activities

The biological potential of any legend is determined by a blend of factors, including *in silico* study of its binding affinity to target proteins PDB: 1DB1 and PDB: 4FA6 with Click docking, its Absorption, Distribution, Metabolism, and Excretion (ADME) properties with star drop version-6.5, and its inhibition efficacy in cell-based MTT assay method. In this study, three isolated compounds A, B, and C, were evaluated for their anticancer properties in human hepatoma cancer cell lines (HepG2) and mouse embryonic fibroblasts normal cell lines (NIH 3T3), with a focus on IC_{50} values and dose-dependent inhibition. Furthermore, *in silico* docking studies were employed to assess each compound's binding affinity to key target proteins and ADME properties, providing deeper insight into their biological profiles.

This comprehensive comparison examines how each compound performs in terms of inhibition efficacy, binding affinity, and amino acid interactions to offer a complete evaluation of their potential for further drug development, especially for human hepatoma cancer cells (HepG2) and mouse embryonic fibroblast normal cells (NIH 3T3). Ultimately, the analysis will help determine which compound holds the most promise for therapeutic use and the reasons for this.

In silico docking study

In this study, we compare the docking results of three compounds (A, B, and C) against two targets: PDB: 1DB1, a protein associated with cancer, and PDB: 4FA6, which is involved in hepatoprotection. We will also compare these compounds to standard drugs, such as vitamin D and pyrrolidinyl-pyrido-pyrimidinone derivatives (Mehra et al., 2016; Al-Warhi et al., 2021), highlighting their roles as kinase inhibitors that target critical pathways, including PI3K/Akt/mTOR and cyclin-dependent kinases (CDKs), both of which are associated with potent anticancer and hepatoprotective activities. The docking results are given in **Tab. 4**.

The docking scores of isolated compounds A and B (-9.50 and -9.44, respectively) are quite similar, indicating a strong binding affinity to PDB: 1DB1, compared with isolated compound C which has a weaker docking score (-7.14). This suggests that both compounds A and B could potentially have a good therapeutic effect, particularly in terms of their anticancer activity. Compounds A and B display interactions with Leu-230, Leu-233, Val-234, Ile-271, Trp-286, Tyr-295, His-305, His-397 amino acid residues in the binding pockets. Compound B has two more interactions with Leu-313 and Val-418 amino acid residues. Compound C shows interactions with Pro-145, Tyr-147, Asn-276, and Glu-277 amino acid residues in the binding pockets. Standard drug (vitamin D) demonstrated interactions with Tyr-143, Leu-233, Val-234, Ser-237, Arg-274, Ser-275, Ser-278, Trp-286, His-305, Ser-306, Ser-314, His-397, Arg-391 amino acid residues in the binding pockets. The interactions between compounds A and B with the amino acid residues in the binding

Table 4. Docking study of isolated compounds against protein associated with cancer (PDB: 1DB1) and hepatoprotection (PDB: 4FA6)

S.No	Compound Code	Docking score and Amino acid residue interactions			
		PDB: 1DB1		PDB: 4FA6	
1	**A**	-9.50	Leu-230, Leu-233, Val-234, Lle-271, Trp-286, Tyr-295, His-305, His-397	-8.13	Pro-563, Ser-594, Gln-629
2	**B**	-9.44	Leu-227, Leu-230, Val-234, Lie-271, Lie-268, Trp-286, His-305, Leu-313, Val-418	-8.42	Pro-563, Lew-564, Asp-632, Ser-1032, Ser-1044
3	**C**	-7.14	Pro-145, Try-147, Asn-276, Glu-277, Leu-320, Leu-325, Glu-327, His-330	-8.54	Pro-563, Ser-594, Gln-629
4	**Standard**	-9.76	Tyr-143, Leu-233 Val-234, Ser-237 Arg-274 ,Ser-275 Ser-278, Trp-286 His-305, Ser-306 Ser-314, His-397 Arg-391	-10.84	Lys 802, Asp 810, Val 822, Lys 833, Val 851 and Asp 933

pocket suggest a strong binding that likely involves hydrophobic and aromatic interactions, which are crucial for the stability of protein-ligand complexes. The presence of Tyr-295 in both compounds A and B also highlights aromatic interactions, which are common in anticancer drugs due to their ability to stabilize interactions and interfere with key protein functions involved in tumor progression. Compound B has additional interactions with Leu-313 and Val-418, which may contribute to higher specificity and potentially fewer off-target effects, making it a more selective and effective compound. These residues are likely involved in more specific interactions, which could improve the overall pharmacokinetic profile, reducing systemic toxicity. Compound C, in contrast, interacts with Pro-145, Tyr-147, Asn-276, and Glu-277, suggesting that its interactions are less stable and more flexible due to the presence of proline, a residue known for introducing flexibility in protein structures. The interactions involving proline could result in reduced specificity, leading to weaker binding compared to compounds A and B.

For the hepatoprotective properties of isolated compounds, docking studies were carried out against PDB; 4FA6. Compounds A, B, and C demonstrated -8.13, -8.42, and -8.54, respectively, revealing that compound C has a stronger docking score than the other two compounds. This suggests that compound C might have a stronger potential for hepatoprotective activity compared to the other two compounds. Compounds A and C display interactions with Pro-563, Ser-594, and Gln-629 amino acid residues in the binding pockets. Compound B shows interactions with Pro-563, Leu-564, Asp-632, Ser-1032, and Ser-1044 amino acid residues in the binding pockets. Standard drug (Pyrrolidinyl Pyrido Pyrimidinone Derivatives) demonstrated interactions with Lys-802, Asp-810, Val-822, Lys-833, Val-851, and Asp-933 amino acid residues in the binding pockets. Compound C stands out due to its stronger docking score against PDB: 4FA6. This could make it a strong candidate for protecting liver cells from damage, although its weaker binding to PDB: 1DB1 means it might not be as effective against cancer. The virtual screening of isolated compounds against VDR (PDB: 1DB1) and PI3Ka domain (PDB: 4FA6) and their 3D amino acid residue interaction are given in **Fig. 4** and **Fig.**

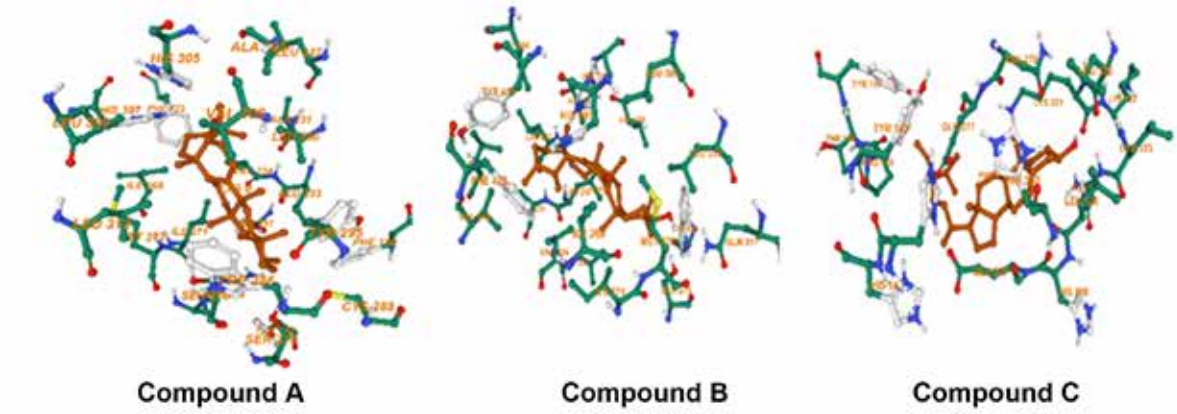

Fig. 4. Isolated compounds from the virtual screening (PDB: 1DB1) and their 3D interaction diagram specifying the amino acid residue interaction of the compound with the binding pocket of the Vitamin D Receptor domain (VDR)

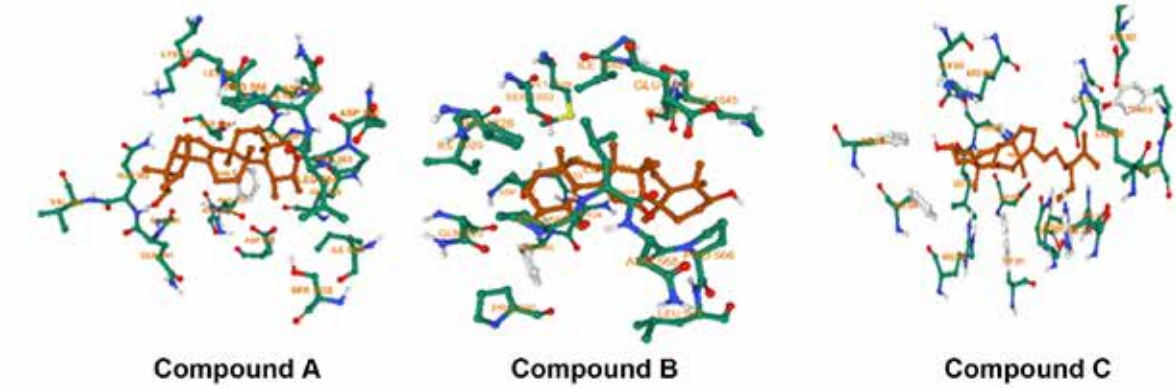

Fig. 5. Isolated compounds from the virtual screening (PDB: 4FA6) and their 3D interaction diagram specifying the amino acid residue interaction of the compound with the binding pocket of the PI3Ka domain

5.

In silico ADME Study

The *in silico* study of Absorption, Distribution, Metabolism, and Excretion (ADME) properties displays key parameters related to oral bioavailability, CNS penetration, drug-likeness, and transport interaction characteristics. *In silico* ADME properties study results of the isolated compound are given in **Tab. 5**. The Oral Non-CNS Scoring Profile evaluates the likelihood of the compound being orally bioavailable and not penetrating the central nervous system (CNS). Higher scores indicate better oral bioavailability and reduced CNS penetration. Compound B has the highest score (0.08156), suggesting it is more likely to be orally bioavailable and less likely to cross the blood-brain barrier (BBB). Compound A has a moderate score (0.06833), implying good oral absorption and low CNS penetration. Compound C has the lowest score (0.03972), which might indicate a lower potential for oral bioavailability and possibly higher CNS penetration compared to A and B. The logS value indicates water solubility, with higher values suggesting better solubility. Water solubility plays a crucial role in absorption. Compound B has the highest logS, indicating it is the most water-soluble and, therefore, likely to have better absorption characteristics. LogP reflects the compound's lipophilicity, crucial for membrane permeability and distribution. Compounds with high logP values tend to cross cellular membranes more easily but may have issues with solubility. Compound C is the most lipophilic, which could indicate it has a higher tendency to accumulate in tissues but might also pose challenges for solubility and gastrointestinal absorption. Compound B is less lipophilic and might have lower tissue accumulation, but its moderate lipophilicity also suggests a balanced absorption profile. The pKi value represents the binding affinity to the cytochrome P450 enzyme (specifically CYP2C9). Higher pKi values indicate stronger inhibition, which can lead to drug-drug interactions. Compounds A and B show similar, moderately strong inhibition of CYP2C9, which might indicate potential for drug-drug interactions, particularly in metabolism. The hERG inhibition is a critical factor in assessing the potential for arrhythmia caused by drugs (QT interval prolongation). The pIC_{50} value reflects the compound's affinity for the hERG channel (higher is worse). Compound C demonstrates the highest hERG pIC_{50}, indicating it is the most likely to inhibit hERG, which raises concerns about cardiovascular safety. Compound A has a moderate hERG pIC_{50}, which could indicate a lower risk of arrhythmia but still warrants caution. The BBB log

Table 5. *In silico* ADME properties study of isolated compounds

Compound ID	Oral Non CNS Scoring Profile_ Score	Log-S	2C9 pKi	hERG pIC_{50}	BBB log([brain]:[blood])	HIA category_ Probability	P-gp category_ Probability	Lipinski's Rule of Five Parameter			
								M.Wt. (<500)	LogP (<5)	H-bond donor (<5)	H-Bond acceptor (<10)	Violation
A	0.06833	0.7458	5.02	5.314	0.5998	-"" = 0.0371353;""+"" = 0.962865	no"" = 0.71;""yes"" = 0.29	426.7	6.06	1	1	1
B	0.08156	0.8872	5.03	4.914	0.07338	-"" = 0.0371353;""+"" = 0.962865	no"" = 0.75;""yes"" = 0.25	440.7	5.376	1	2	1
C	0.03972	0.2406	4.949	5.894	0.6824	-"" = 0.0371353;""+"" = 0.962865	no"" = 0.68;""yes"" = 0.32	414.7	7.117	1	1	1

([brain]:[blood]) ratio indicates the potential for the compound to cross the blood-brain barrier. Higher values suggest better penetration into the brain. Compound C has the highest value, suggesting it is the most likely to penetrate the BBB and reach the CNS, which might limit its suitability for CNS-safe drug targets. Compound A has a moderate BBB penetration potential, which is balanced for drugs that should remain outside the CNS. Compound B has the lowest BBB ratio, indicating it is the least likely to cross the blood-brain barrier, which may be beneficial for drugs intended for non-CNS targets. All compounds have the same high probability (96.3%) of good human intestinal absorption. This suggests that all three compounds are likely to be well absorbed in the gastrointestinal tract, assuming other factors (e.g., solubility, permeability) are favorable. P-glycoprotein (P-gp) is a transporter that can efflux drugs out of cells, reducing bioavailability. The probabilities suggest that P-gp interaction is less likely for all three compounds, but compounds A and B have a higher likelihood of being substrates for P-gp (29% and 25% chance, respectively), which could reduce their bioavailability or complicate drug interactions. Compound C is less likely to be a P-gp substrate (32% chance). All the isolated compounds were in violation of Lipinski's rule (i.e., the log P value is >5), indicating that compounds have more lipophilicity, which is crucial for membrane permeability and distribution.

Cell line study

All three isolated compounds (A, B, and C) demonstrated dose-dependent inhibition in NIH 3T3 cells. Compound A displayed inhibition against the NIH 3T3 cell line, with a percentage of 23.61% at 63 µg/mL increasing to 47.34% at 1000 µg/mL, and the IC_{50} at 1068 µg/mL. The results of *in vivo* cytotoxicity screening of isolated compounds against HepG2 and NIH 3T3 cell lines are given in **Tab. 6**.

Compound B inhibition against the NIH 3T3 cell line started at 23.15% at 63 µg/mL and increased to 46.99% at 1000 µg/mL, IC_{50} at 1153 µg/mL. Compound C demonstrated inhibition against the NIH 3T3 cells line from 18.75% at 63 µg/mL to 46.06% at 1000 µg/mL with an IC_{50} at 1310 µg/mL. On the other hand, inhibition against HepG2 cells line study, Compound A shows a steeper increase in inhibition with increasing concentration in HepG2 cells at 25.82% at 63 µg/mL and rises to 67.54% at 1000 µg/mL, which IC_{50} of 455 µg/mL. Compound B rises from 20.21% at 63 µg/mL to 60.98% at 1000 µg/mL with IC_{50} of 538 µg/mL. Compound C displayed inhibition starting at 22.20% at 63 µg/mL and reached 55.49% at 1000 µg/mL, with an IC_{50} at 556 µg/mL. Compound A exhibits greater inhibition against HepG2 liver cancer cells than against NIH 3T3 fibroblasts, suggesting that it is more effective at lower doses for cancer cells and indicates selectivity for cancerous cells, which is a crucial characteristic for anticancer agents, as it helps reduce toxicity to normal tissues. Compounds B and C are also more effective against HepG2 cells than NIH 3T3 cells, with a steeper inhibition curve for HepG2. However, later, both compounds' potency is slightly lower than compound A's in both cell lines.

Conclusion

Compound A demonstrates the strongest overall potency, particularly for HepG2 liver cancer cells, with -9.50 against cancer protein (PDB: 1DB1), suggesting robust binding and pharmacological potential. However, its potential cardiovascular risks and CNS penetration may require optimization before being widely used. Compound A shows dual-target activity and favorable binding affinity to both anticancer activity (PDB: 1DB1) and hepatoprotective properties (PDB: 4FA6). Its more predictable pharmacokinetic profile and selective binding make it an excellent candidate for non-CNS drug development, particularly in the context of liver cancer therapy. Compound C has the weakest binding to PDB: 1DB1, but its stronger binding to

Table 6. *In vivo* cytotoxicity screening of isolated compounds against HepG2 and NIH 3T3 cell line

Concentration (µg/mL)	% inhibition of Compound A		% inhibition of Compound B		% inhibition of Compound C	
	NIH 3T3	HepG2	NIH 3T3	HepG2	NIH 3T3	HepG2
63	23.61	25.82	23.15	20.21	18.75	22.2
125	34.26	30.26	33.10	25.35	28.24	29.66
250	39.35	41.2	38.31	33.87	33.91	35.68
500	44.33	50.61	43.29	44.27	39.93	46.27
1000	47.34	67.54	46.99	60.98	46.06	55.49
IC_{50} Values	1068	455	1153	538	1310	556

PDB: 4FA6 suggests potential for CNS-targeted therapies. However, its overall potency is the lowest, and its solubility, lipophilicity, and cardiovascular concerns require significant optimization. Compound B is the most promising candidate for further development, particularly for liver cancer therapies. Compound A remains a strong candidate but requires optimization to address potential CNS penetration and cardiovascular issues. Compound C requires extensive modifications to improve its potency, selectivity, and safety profile before it can advance in drug development.

Acknowledgements. The authors would like to thank the School of Biotechnology, National Institute of Technology, NIT Campus P.O. 673601, Kozhikode, Kerala, India; Dr. A. Santhiagu, Professor, School of Biotechnology, NITC, Calicut, and KMCH College of Pharmacy, Coimbatore for their kind support of my research studies.

References

Aarthi, V., Shakila, R., Sasikala, E., & Pitchiahkumar, M. (2014). Pharmacognostical studies on *Ehretia microphylla* Lamk. *Asian Journal of Traditional Medicines*, *9*(5), 118-129. https://www.researchgate.net/publication/270957123

Al-Warhi, T., Aljaeed, N., El-Brollosy, N., Alam, M.M., Almutairi, M.S., Iqbal, M.N., & Ghabbour, H.A. (2021). Design, synthesis and anticancer evaluation of novel pyrido[2,3-d]pyrimidinone derivatives as dual PI3K/mTOR inhibitors. *European Journal of Medicinal Chemistry*, *213*, 113160. https://doi.org/10.1016/j.ejmech.2021.113160

Cagampan, D.M., Lacuata, K.A., Ples, M.B., & Vitor II, R.J.S. (2018). Effect of *Ehretia microphylla* on the blood cholesterol and weight of ICR mice (*Mus musculus*). *National Journal of Physiology, Pharmacy and Pharmacology*, *8*(7), 983-987. https://doi.org/10.5455/NJPPP.2018.8.0206804032018

Chen, M.F., Chen, P.T., Lu, M.S., Chen, W.C., Lin, P.Y., & Lin, Y.S. (2022). Role of vitamin D3 in tumor aggressiveness and radiation response for hepatocellular carcinoma. *Journal of Gastroenterology and Hepatology*, *37*(6), 1096-1105. https://doi.org/10.1111/jgh.15882

Chiang, K.C. & Chen, T.C. (2011). Hepatocellular carcinoma and vitamin D: A review. *Journal of Gastroenterology and Hepatology*, *26*(10), 1597-1603. https://doi.org/10.1111/j.1440-1746.2011.06892.x

Jain, A., Singhai, A.K., & Dixit, V.K. (2006). A comparative study of ethanol extract of leaves of *Tephrosia purpurea* Pers and the flavonoid isolated for hepatoprotective activity. *Indian Journal of Pharmaceutical Sciences*, *68*(6), 740-743. https://doi.org/10.4103/0250-474X.31006

Jeganathan, N.S. & Kannan, K.H. (2008). HPTLC method for estimation of ellagic acid and gallic acid in *Triphala churanam* formulations. *Research Journal of Phytochemistry*, *2*(1), 1-9. https://doi.org/10.3923/rjphyto.2008.1.9

Jiang, S., Wang, M., Kaur, A., Jiang, L., Cai, Y., Luo, J., Li, M., Wang, H., Wan, D., & Peng, Y. (2024). *Ehretia* genus: A comprehensive review of its botany, ethnomedicinal values, phytochemistry, pharmacology, toxicology and clinical studies. *Frontiers in Pharmacology*, *16*, 1-25. https://doi.org/10.3389/fphar.2025.1526359

Mahrath, A.J., Hassan, G.S., & Obaid, E.K. (2015). Isolation and characterization of terpenoid derivatives from medicinal plant roots by thin layer and flash column chromatography (TLC & FCC) techniques. *International Journal of Chemical Sciences*, *13*(2), 983-989. https://doi.org/10.13140/RG.2.1.2428.3684

Maurya, H.K. (2014). Natural and synthetic molecular medicine in cancer research: A review. *Journal of Cancer Research and Molecular Medicine*, *1*(1), 101. https://www.researchgate.net/publication/276067533

Mawa, S., Jantan, I., & Husain, K. (2016). Isolation of terpenoids from the stem of *Ficus aurantiaca* Griff and their effects on reactive oxygen species production and chemotactic activity of neutrophils. *Molecules*, *21*(1), 9. https://doi.org/10.3390/molecules21010009

Mcule. (n.d.). 1-Click Docking. Retrieved May 19, 2020, from https://mcule.com/apps/1-click-docking/

Mehra, R., Rajput, V.S., Gupta, M., Chib, R., Kumar, A., Wazir, P., Khan, I.A., & Nargotra, A. (2016). Benzothiazole derivative as a novel *Mycobacterium tuberculosis* shikimate kinase inhibitor: Identification and elucidation of its allosteric mode of inhibition. *Journal of Chemical Information and Modeling*, *56*(5), 930-940. https://doi.org/10.1021/acs.jcim.6b00056

Monks, A., Scudiero, D., Skehan, P., Shoemaker, R., Paull, K., Vistica, D., Hose, C., Langley, J., Cronise, P., Vaigro-Wolff, A., Gray-Goodrich, M., Campbell, H., Mayo, J., & Boyd, M. (1991). Feasibility of a high-flux anticancer drug screen using a diverse panel of cultured human tumor cell lines. *Journal of the National Cancer Institute*, *83*(11), 757-766. https://doi.org/10.1093/jnci/83.11.757

Mosmann, T. (1983). Rapid colorimetric assay for cellular growth and survival: Application to

proliferation and cytotoxicity assays. *Journal of Immunological Methods*, *65*(1-2), 55-63. https://doi.org/10.1016/0022-1759(83)90303-4

Palaniappan, R., Senguttuvan, J., Kandasamy, P., & Subramaniam, P. (2014). *In vitro* antioxidant properties of the traditional medicinal plant species, *Ehretia microphylla* Lam. and *Erythroxylon monogynum* Roxb. *Research Journal of Pharmaceutical, Biological and Chemical Sciences*, *5*(1), 247-252.

Pooja, S., Shri, R., & Kumar, S. (2022). Phytochemical and *in vitro* cytotoxic screening of chloroform extract of *Ehretia microphylla* Lamk. *Stresses*, *2*(4), 384-394. https://doi.org/10.3390/stresses2040027

Sajeeth, C.I., Manna, P.K., Manavalan, R., & Jolly, C.I. (2010). Quantitative estimation of gallic acid, rutin and quercetin in certain herbal plants by HPTLC method. *Der Chemica Sinica*, *1*, 80-85.

Shamsan, E., Almezgagi, M., Gamah, M., Khan, N., Qasem, A., Chuanchuan, L., & Haining, F. (2024). The role of PI3k/AKT signaling pathway in attenuating liver fibrosis: A comprehensive review. *Frontiers in Medicine*, *11*, A1389329. https://doi.org/10.3389/fmed.2024.1389329

Sharifi-Rad, J., Ozleyen, A., Tumer, T.B., Adetunji, C.O., El Omari, N., Balahbib, A., Taheri, Y., Bouyahya, A., Martorell, M., Martins, N., & Cho, W.C. (2019). Natural products and synthetic analogs as a source of antitumor drugs. *Biomolecules*, *9*(11), 679. https://doi.org/10.3390/biom9110679

Sharma, P., Shri, R., & Kumar, S. (2022). Phytochemical and *in vitro* cytotoxic screening of chloroform extract of *Ehretia microphylla* Lamk. *Stresses*, *2*(4), 384-394. https://doi.org/10.3390/stresses2040027

Trump, D.L. (2018). Calcitriol and cancer therapy: A missed opportunity. *Bone Reports*, *9*, 110-119. https://doi.org/10.1016/j.bonr.2018.06.002

Umali, F.A.C. & Chua, A.H. (2017). *Ehretia microphylla* (Tsaang Gubat) versus loratadine as treatment for allergic rhinitis: A randomized controlled trial. *Philippine Journal of Otolaryngology - Head and Neck Surgery*, *32*(2), 6-10. https://doi.org/10.32412/pjohns.v32i2.57

Villanueva, A. (2019). Hepatocellular carcinoma. *The New England Journal of Medicine*, *380*(15), 1450-1462.https://doi.org/10.1056/NEJMra1713263

World Health Organization. (2016). *Projections of mortality and causes of death, 2016 to 2060*. http://www.who.int/healthinfo/global_burden disease/projections/en/

Yuan, F., Xu, Y., You, K., Zhang, J., Yang, F., & Li, Y.X. (2021). Calcitriol alleviates ethanol-induced hepatotoxicity via AMPK/mTOR-mediated autophagy. *Archives of Biochemistry and Biophysics*, *697*, 108694. https://doi.org/10.1016/j.abb.2020.108694

Yuvaraja, K.R., Santhiagu, A., Jasemin, S., & Gopalasatheeskumar, K. (2020). Antioxidant potential of medicinally important plants *Ehretia microphylla*, *Dipteracanthus patulus* and *Hydnocarpus laurifolia*. *International Journal of Biology, Pharmacy and Allied Sciences*, *9*(2), 195-205. https://doi.org/10.31032/IJBPAS/2020/9.2.4957

Yuvaraja, K.R., Santhiagu, A., Jasemine, S., & Gopalasatheeskumar, K. (2021). Hepatoprotective activity of *Ehretia microphylla* on paracetamol induced liver toxic rats. *Journal of Research in Pharmacy*, *25*(1), 89-98. https://doi.org/10.35333/jrp.2021.286

Zhang, Z. & Wang, C.Z. (2020). Vitamin D signaling in inflammation and cancer: Molecular mechanisms and therapeutic implications. *Current Medicinal Chemistry*, *27*(24), 4326–4339. https://doi.org/10.2174/0929867326666191009152137